Biomaterials 30 (2009) 4336–4347

Contents lists available at ScienceDirect

Biomaterials

journal homepage: www.elsevier.com/locate/biomaterials

Multifunctional protein-encapsulated polycaprolactone scaffolds: Fabrication and in vitro assessment for tissue engineering

Seher Ozkan [a], Dilhan M. Kalyon [a,*], Xiaojun Yu [a], Craig A. McKelvey [b], Michael Lowinger [b]

[a] Chemical, Biomedical and Materials Engineering Department, Stevens Institute of Technology, McLean Chemical Sciences Building, Castle Point St., Hoboken, NJ 07030, USA
[b] Pharmaceutical R&D, Merck & Co., Inc., West Point, PA 19486, USA

ARTICLE INFO

Article history:
Received 21 January 2009
Accepted 28 April 2009
Available online 28 May 2009

Keywords:
Scaffold
Tissue engineering
Sustained release
Extrusion
Protein delivery

ABSTRACT

Here we demonstrate the use of a twin screw extrusion/spiral winding (TSESW) process to generate protein-encapsulated tissue engineering scaffolds. Bovine serum albumin (BSA) was distributed into PCL matrix using both wet and hot melt extrusion methods. The encapsulation efficiency and the time-dependent release rate, as well as the tertiary structure of BSA (via circular dichroism), were investigated as a function of processing method and conditions. Within the relatively narrow processing window of this demonstration study it was determined that the wet extrusion method gave rise to greater stability of the BSA on the basis of circular dichroism data. The rate of proliferation of human fetal osteoblast (hFOB) cells and the rate of mineral deposition were found to be greater for wet extruded scaffolds, presumably due to the important differences in surface topographies (smoother scaffold surfaces upon wet extrusion). Overall, these findings suggest that the twin screw extrusion/spiral winding (TSESW) process offers significant advantages and flexibility in generating a wide variety of non-cytotoxic tissue engineering scaffolds with controllable distributions of porosity, physical and chemical properties and protein concentrations that can be tailored for the specific requirements of each tissue engineering application.

1. Introduction

Tissue engineering involves in vitro culturing of human cells on biodegradable and preferably bioresorbable scaffolds that provide the necessary structural support, which are then implanted into the human body, where the cells continue to proliferate and differentiate while the underlying scaffold material degrades [1]. This exciting multidisciplinary field is challenged by the complex gradations in cell type and extracellular matrix, ECM, microstructures found in human tissues [2–6]. To meet this challenge tissue engineering scaffolds need to generate spaciotemporal signals to actively communicate with surrounding cells [7], for example, by releasing growth factors as a function of location and time [8]. Recent studies with human mesenchymal stem cells have also indicated that small-molecule functional groups attached to three dimensional substrates can induce selective differentiation of the stem cells suggesting that gradations in the chemical nature of the tissue engineering scaffolds can induce location-dependent changes in the differentiation of stem cells [9]. Furthermore, layered scaffolds can be utilized for gene delivery as demonstrated with encapsulated plasmid [10]. Overall, one major challenge of tissue engineering is the maintenance of the secondary structures of sensitive protein based biological agents that are incorporated into scaffolds [11].

Another challenge of tissue engineering is to translate laboratory-based scaffold preparation processes into "clinically appropriate larger scale production techniques" that are "reproducible, safe, clinically effective and economically acceptable" [12]. It is suggested that the affordable production of tissue engineering materials requires the use of scalable automated systems that generate a product with consistent and reproducible properties at industrially-acceptable production volumes [12]. However, there are currently very few processes which would be able to distribute the requisite biological agents, including growth factors and gene delivery agents, into desired concentration profiles in tissue engineering scaffolds without significant transformation/deterioration of protein structure.

There are currently a limited number of methods used for the fabrication of tissue engineering scaffolds with the ability to disperse proteins including growth factors for selective differentiation of cells proliferated within the scaffold matrix [13–23]. These include emulsion freeze drying [13], high pressure carbon dioxide fabrication [14,23], spray-freeze drying [15], precipitation casting [16], protein-encapsulated microsphere based scaffold manufacturing [17,20–22] and coating scaffolds with protein solutions [18,19]. Here

* Corresponding author. Tel.: +1 201 216 8225; fax: +1 201 216 8306.
E-mail address: dkalyon@stevens.edu (D.M. Kalyon).

0142-9612/$ – see front matter © 2009 Elsevier Ltd. All rights reserved.
doi:10.1016/j.biomaterials.2009.04.050

we are proposing another process for the fabrication of tissue engineering scaffolds for controlled protein release that should offer significant advantages in the areas of precision in the spatial distribution of protein concentrations and flexibility and manufacturability at relatively high scales to enable consistent and reproducible scaffold structures and properties.

The basic process integrates the twin screw extrusion with spiral winding and can be utilized for two different methods of scaffold construction, i.e., first wet extrusion (involving the dissolution of the biodegradable polymeric matrix in an organic solvent) and second melt extrusion (without the solvent). Here we demonstrate the abilities of the process for protein encapsulation and release using polycaprolactone, PCL, as the matrix polymer incorporated with bovine serum albumin, BSA. The effects of processing conditions and porosity on compressive properties, surface topography of the scaffolds and the encapsulation efficiency, release profiles and the secondary structure of BSA are investigated. The biocompatibility of the functionalized scaffolds fabricated via the twin screw extrusion/spiral winding process and their suitability for bone tissue engineering are assessed with an in vitro study employing human fetal osteoblast (hFOB) cells.

2. Experimental

2.1. The twin screw extrusion/spiral winding (TSESW) process for scaffold fabrication and materials

The TSESW process integrates the twin screw extrusion process with a modified filament winding method (designated here as "spiral winding"). The twin screw extrusion part of the process enables the carrying out of multiple unit operations including solids' conveying, melting, temperature control, distributive and dispersive mixing of particles and nanoparticles, deaeration and shaping of the biocomposite. The feeding of the solid and liquid ingredients in a time-dependent fashion can also generate spatial gradations in composition and porosity of the extrudates, which are subsequently wound around a mandrel that concomitantly rotates and translates sideways creating a helical and spiral trajectory for the fabrication of cylindrical extrudates (Fig. 1). The technology has the capability to generate radially and axially graded tissue engineering scaffolds by time-dependent variations in the feeding rates of various ingredients and the operating variables of the process including temperatures, winding rotational and translation speeds. Furthermore, the TSESW method is amenable to large-scale manufacturing and is suitable for handling polymers, solutions and gels under different temperature conditions, e.g. wet or melt extrusion.

The focus of this study is on the demonstration of the protein dispersion and encapsulation capabilities of the process and the effects of such encapsulation on the release rate and the stability of encapsulated proteins. Both the melt and wet extrusion methods were undertaken, i.e., seven sets of BSA encapsulated porous scaffold samples were fabricated using wet or melt extrusion to investigate the effects of changes in process conditions, namely the flow rate (and hence the residence time) and temperature (in the case of melt extrusion) on the secondary structure of the dispersed protein. Scaffolds with changing porosity distributions were also fabricated to alter protein encapsulation efficiency and sustained release profiles on one hand and the development of the compressive properties on the other. Three types of scaffolds were also subjected to the analysis of the cell/scaffold interactions using hFOB cells.

In the TSESW process a 7.5 mm mini twin screw extruder (Material Processing & Research, Inc., Hackensack, NJ) with a rectangular slit die (width 10 mm and gap 1 mm) was used in conjunction with a mandrel with a diameter of 1.5 mm, placed orthogonal to the extrusion direction (Fig. 1a). The twin screw extruder has the capability to control temperatures over multiple zones, a feature which is generally not possible with conventional and rapid prototyping/fiber deposition type scaffold manufacturing methods. A rotating mandrel is placed at an angle to the extrusion direction to allow the winding of the extrudate on the mandrel surface (Fig. 1a). The mandrel is rotated as well as translated in the transverse to extrusion direction to control the helix angle of the trajectory of the extrudate, wound around the mandrel and to set the thicknesses of the successive layers of the scaffold. The inner diameter of the scaffold can be decreased or increased simply by decreasing or increasing the mandrel diameter, respectively. There is no upper limit to the outside diameter of the scaffold. The inner and the outer diameters and the length of the scaffolds can generally be controlled within ±0.5–2%.

In our demonstration experiments polycaprolactone (PCL) pellets (with number average molecular weight of 80 kDa and available from Sigma Aldrich, Milwaukee, Wisconsin) were milled under cryogenic conditions. The particle size of the milled powder was characterized by a laser diffraction particle size analyzer (Sympatec, Helos) and was determined to exhibit a narrow distribution around 200 μm. After milling the PCL powder was coated with 5 wt% bovine serum albumin, BSA (Sigma, USA) in a wet granulator (DIOSNA Wet granulator). Coated particles were dried in vacuum oven at 37 °C and kept in a sealed container at 4 °C until further usage. The homogeneity of BSA distribution was assessed by removing 100 mg specimens from the dried powder and dissolving the BSA coating in phosphate buffer saline, PBS, at room temperature. The concentration of the recovered BSA in PBS was measured using UV spectrophotometry at 280 nm wavelength with a 10 mm path length cuvette (HP8453 UV/Vis). Coated BSA amount was found to be 4.8 ± 0.6% by weight.

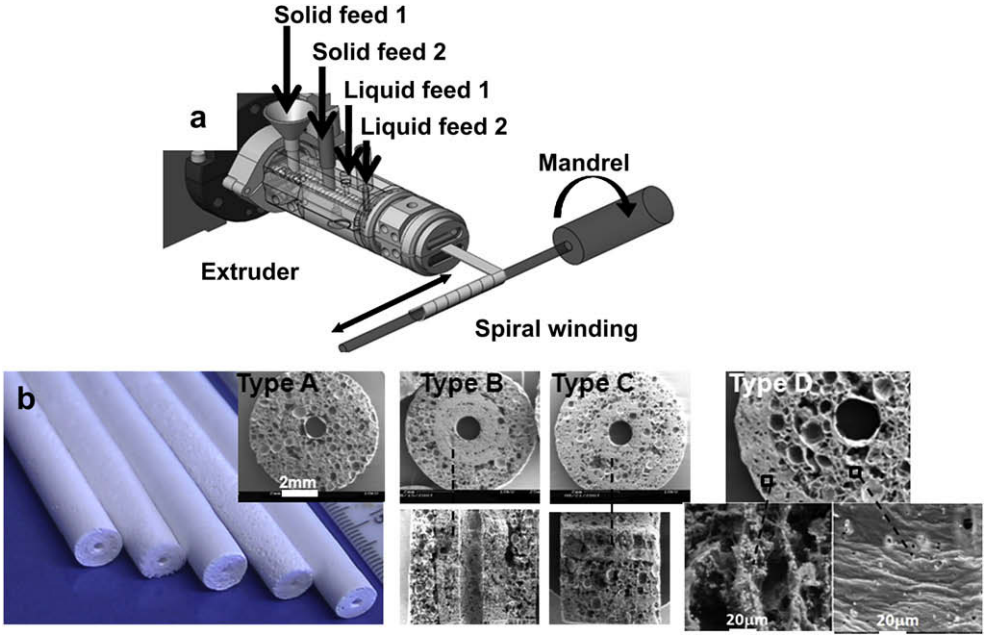

Fig. 1. Schematics of twin screw extrusion/spiral winding process (TSESW) showing multiple solid and liquid feed ports, extruder barrel, slit die and extrudate coming out of die and being wrapped around the mandrel (a). Typical functionally-graded scaffolds fabricated via TSESW process (b). Single layer scaffolds with homogeneous pore size and material concentration (Type A), multilayered scaffolds with different porosity and constant material concentration at each layer (Types B and C) and multilayered nanocomposite scaffolds with different porosity and different material concentration at each layer (Type D).

2.1.1. Wet extrusion

BSA-coated PCL powder was dissolved in dichloromethane, DCM (Pharmco, USA). The selection of the solvent was based on various stability and other criteria (to be elucidated later). A syringe pump (Harvard Apparatus) was used to feed the BSA incorporated PCL/DCM solution into the twin screw extruder. A loss-in-weight solids' feeder (Brabender Technologies, Mississauga, Canada) was used to feed the porogen NaCl particles which exhibited a broad size distribution in the 10–600 μm range (as determined with a Sympatec, Helos laser diffraction based particle size analyzer). The wet extrusion process was carried out under ambient temperature.

2.1.2. Melt extrusion

PCL powder loaded with BSA was blended with 200 μm size PEO powder (Dow Chemicals, M_n 2000 kDa) at a ratio of 6:4 before feeding it into the twin screw extruder. Particle size of PEO powder was measured using a laser diffraction particle size analyzer (Sympatec, Helos). PEO was added into the mixture as a second porogen to increase the porosity of the final product and decrease the viscosity of the molten polymer/solid particle mixture inside the extruder during the extrusion process. Two loss-in-weight solids' feeders (Brabender Technologies, Mississauga, Canada and K-Tron International, Inc., NJ, USA) were used for feeding of the BSA/PCL/PEO powder blend and the NaCl powder streams into the twin screw extruder. Melt extrusion was carried out at two different processing temperatures of 80 and 100 °C.

The capabilities of the twin screw extrusion/spiral winding (TSESW) process for generating different types of multilayered scaffolds are demonstrated in Fig. 1. For the evaluation of the protein encapsulation capability of the TSESW process Type A scaffolds (homogeneous porosity and protein concentration) were used in conjunction with both wet and melt extrusion with variations in porogen concentrations and processing temperatures for melt extrusion. Sample designations, fabrication method and processing data such as barrel and die temperatures, pressure drop through the die, the torque exerted on the screws (integral of the shear stress distribution on the screw surfaces) are shown in Table 1. Wet extruded samples, i.e., those processed in the presence of dichloromethane, DCM at room temperature, generated negligible pressure drop at the die (<10 psi). Melt extruded samples were processed at two different processing temperatures, 80 and 100 °C without using a chemical solvent. Relatively high pressure values, in the range of 800–1230 psi at the slit die, were observed.

The inner and outer diameters of the wet and melt extruded scaffolds were kept at 1.5 and 8 mm, respectively. The total lengths of the scaffolds were 50 mm for the melt extruded samples and 100 mm for wet extruded samples. After extrusion, the wet extruded samples were dried for 48 h to remove their DCM solvent. Both the wet and melt extruded samples were immersed in deionized water for 170 h (with the water phase changed every 8 h) to leach out the salt and PEO porogens. Sample designations of fabricated scaffolds and their various properties are given in Table 1.

2.2. Scaffold characterization

The porosity values of the PCL/BSA scaffolds were determined on the basis of the geometry and apparent density values of the scaffolds and were verified using Hg intrusion porosimetry with a filling pressure range of 0–420 MPa (Poremaster 60, Quantachrome Instruments, Boynton Beach, FL). In Hg porosimetry the porosity, ϵ, values were determined from the total Hg intrusion volumes, V_i:

$$\epsilon = V_i/(V_i + 1/\rho_{TRUE}) \quad (1)$$

where ρ_{TRUE} is the density of the porous scaffold as measured using He pycnometry (AccuPyc 1330, Micrometrics, Norcross, GA).

A differential scanning calorimeter (DSC-Q50, TA Instruments, USA) was used to measure the bulk crystallinity values of the scaffolds. Sample weights were in the 5–10 mg range. In the DSC experiments the scaffold samples were scanned from 0 to 150 °C at a heating rate of 15 °C/min, using nitrogen as the purge gas. The degree of crystallinity, X_c, values of the scaffolds were obtained from the ratio of the heat of fusion, ΔH_f, values of the PCL (determined from the first heating of the scaffold sample) to the heat of fusion value of pure crystalline PCL, ΔH_c, which is 136 J/g [24].

$$X_c = \Delta H_f/\Delta H_c \quad (2)$$

A LEO Gemini 982 scanning electron microscope equipped with a field emission column was employed for SEM imaging of the scaffold samples prior to and after the culturing of the cells with acceleration voltages ranging from 5 kV to 10 kV. Energy dispersion X-ray (EDX) and energy dispersive spectroscopy (EDS) were conducted upon scanning for 150 s duration at 10 kV to validate the presence of Ca and P deposition by hFOB cells after different incubation periods. Some of the scaffold samples were dipped into liquid nitrogen for 5 min and then fractured in the transverse to flow direction in order to expose the pore morphology and interconnectivity. All samples were sputter coated with about 20 nm of Au and Pd (using an SPI Module sputter coater).

Compression testing of the specimens was performed in the strain range of 0–10% at 0.02 mm/min. Specimens were squeezed until a normal force of 3 g is reached to assure full contact, after which the test was initiated. A dynamic mechanical analysis equipment (RSA III, TA instruments) was used to perform the compression test. The compression samples were 7–8 mm in outer diameter, 1.5 mm in inner diameter and 7–8 mm in length. The compressive stress versus strain data were analyzed from load–displacement measurements and the modulus of elasticity and compressive yield strength values were determined according to ASTM 695-02a.

2.3. Protein encapsulation efficiency

Protein encapsulation efficiency was determined using the method of Tice and Gilley [25]. The BSA encapsulated porous scaffold samples were first completely dissolved in dichloromethane. Second 2 mL of phosphate buffer saline solution (pH 7.4) was added and the system was vigorously mixed and left to rest to phase separate for 4 h. Finally, the supernatant aqueous phase was removed and its concentration of BSA was measured using Bradford protein assay (Quickstart from BioRad). In the Bradford protein assay, 150 μl sample solution and 150 μl Bradford reagent were taken (in triplicate) and added to a 96-well plate and plate was incubated at 37 °C for 10 min in the dark room. Absorbance was measured at 595 nm in conjunction with a SYNERGY HT plate reader (KC4, BIO-TEK, USA). Data was compared to known BSA standards between 0.03 and 0.6 mg/mL to calculate the BSA concentration in the sample. BSA encapsulation efficiency was determined from:

$$\text{BSA encapsulation efficiency} = 100 \times (\text{measured BSA amount}/\text{theoretical maximum loaded BSA amount})$$

2.4. In vitro BSA release study

In vitro BSA release tests were carried out for both wet and melt extruded porous scaffold samples. The porous tubular scaffolds were cut into 5 mm long specimens (70–90 mg depending on their porosity). Approximately 200 mg of scaffold samples (210 mg samples from W3 and 180 mg from W1, W2, M3 and 190 mg W4, M1, M2) were placed into standard 24 well plates and soaked in 1 mL PBS. The samples were kept in a humidity and temperature controlled sterile incubator at 37 °C. At various intervals the supernatant arising from each well was collected and replaced with an equal amount of fresh PBS. The concentration of BSA in collected release samples was measured using Bradford protein assay as explained in Section 2.3 (Quickstart from BioRad). Absorbance was measured in 96-well plates at 595 nm using a SYNERGY HT plate reader (KC4, BIO-TEK, USA).

2.5. Analyzing the secondary structure of protein released from PCL scaffolds

The effect of processing conditions on BSA secondary structure was characterized using circular dichroism (CD) under far-UV (JASCO J-810 Spectropolarimeter) in the wavelength range of 160–200 nm using a 0.2 mm path length quartz cell at 25 °C at a scanning speed of 10 nm/min. The CD spectra are obtained from five scans and corrected for PBS buffer signal contribution measured under identical conditions. The protein concentrations of the samples were measured before and after the CD measurements using UV spectrophotometry at 280 nm wavelength with a 10 mm

Table 1
Scaffold designation and their various processing conditions and properties.

Sample designation	W1	W2	W3	W4	M1	M2	M3
Fabrication method	Wet extrusion	Wet extrusion	Wet extrusion	Wet extrusion	Melt extrusion	Melt extrusion	Melt extrusion
Processing temperature, °C	25	25	25	25	80	100	100
Die pressure, psi	10	10	10	10	1230	800	1230
Torque, %	14	15	16	13	36	20	36
Shear stress at the slit die wall, kPa	1.138	1.138	1.138	1.138	139.942	91.019	139.942
Apparent shear rate at the slit die, 1/s	5.508	5.738	5.969	5.201	3.282	3.282	4.050
Porosity, %	75.1 ± 0.4	78.6 ± 0.7	80.1 ± 0.1	68.9 ± 0.8	69.1 ± 1.7	74.2 ± 1.3	77.2 ± 0.5
Young's modulus, E, kPa	48.2 ± 2.1	33.3 ± 8.4	30 ± 2	80.8 ± 4.1	63.8 ± 10.6	44.2 ± 11	38 ± 1
Yield stress, σ, kPa	372.5 ± 30	320 ± 59	250 ± 10	748 ± 73	–	440 ± 65	330 ± 87
Bulk crystallinity, %	44.6 ± 3	49.6 ± 3	43.1 ± 4	47.6 ± 3	48.4 ± 1	44 ± 1	44.9 ± 1
BSA encapsulation efficiency, %	33	29	34	59	38	33	28

path length cuvette (HP8453 UV/vis) and Bradford protein assay. The CD spectra were normalized for the protein concentration. CDPro software was used to calculate the percentages of the α-helix and β-sheet of BSA.

2.6. Cell–scaffold interactions

In order to evaluate the biocompatibility of the scaffolds fabricated by TSESW method a cell culturing study was carried out using melt and wet extruded scaffold specimens (W1, W3 and M3). Scaffold specimens were divided into 2.5 mm long sections. They were sterilized upon being kept immersed in 70% ethanol for 2 h. The scaffolds were then washed with phosphate-buffered saline (PBS) several times to remove the ethanol, followed by exposure to UV light for 30 min following Yu et al. [26]. The sterilized scaffolds were kept in complete growth medium until cell culturing.

Human fetal osteoblast (hFOB) cells were used for the assessment of the biocompatibility of the scaffolds. The hFOB cells were selected for culturing due to their relatively high growth rates and rapid differentiation into mature osteoblasts [27–33]. HFOB cells, which were obtained from American Type Culture Collection (ATCC, USA – designation hFOB 1.19), were passaged once a week in T-75 culture flasks and cultured in complete growth medium containing a 1:1 mixture of Ham's F12/Dulbecco's modified Eagle's medium without phenol red with stable glutamine (PromoCell), 0.3 mg/mL of Geneticin (G418) (Cellgro, USA), 10% fetal bovine serum (Atlanta Biologics), 100 μg/mL penicillin and 100 mU/mL streptomycin (Atlanta Biologics). Cultures were grown at 37 °C in a humidified 5% CO_2 atmosphere. Media were changed every two days and cultures were passaged with 2.5 g/l trypsin (mass fraction 0.25%) and 1 mmol/l EDTA (Gibco, Invitrogen Corporation, USA). After nine passages in complete growth medium, cultures of 90% confluent cells were trypsinized, washed with phosphate-buffered saline (PBS) (ATCC) and centrifuged at 800 rpm for 4 min. Centrifuged hFOB cells were re-suspended in fresh complete growth medium. Following the formation of a dispersed cell suspension, cells were counted with a hemocytometer.

200 μl cell suspension containing 10^5 cells was seeded onto the external and internal surfaces of the PCL scaffold using a micropipette. The scaffolds were flipped a number of times during seeding. After waiting 4 h to allow the hFOB cells to attach onto the scaffold surfaces, 1 mL of complete growth medium was added into each well. The number of cells attached to the surfaces of the scaffolds 24 h later was determined to be in the range of 30,000–50,000 cells/scaffold.

After 3 days of incubation, the complete growth medium was replaced with differentiation medium, which contained 50 μM ascorbic acid (Sigma), 10 mM β-glycerophosphate (Sigma) and 100 nM dexamethasone (Sigma). The scaffolds were incubated for 56 days. Differentiation medium was replaced every 4 days.

2.6.1. Cell viability and proliferation

The cell viability and proliferation rates were assessed using the MTS assay (CellTiter96™ AQueous Assay, Promega, USA), following the CellTiter96™ application procedure. Assay medium was transferred into a 96-well assay plate and the absorbance was measured at 490 nm using a SYNERGY HT plate reader (KC4, BIO-TEK, USA).

2.6.2. Alizarin Red calcium quantification

Mineralized matrix synthesis of hFOB cells on the scaffold specimens was analyzed using the Alizarin Red staining method for Ca^{2+} deposition [26,34]. The scaffold specimens were fixed with 4% paraformaldehyde at 4 °C for 24 h and then stained with 1% Alizarin Red (Sigma) solution for 2 min. After washing five times with distilled water, the red matrix precipitate was solubilized in 10% cetylpyridinium chloride (Sigma), and the optical density of the solution was read at 570 nm with a SYNERGY HT plate reader (KC4, BIO-TEK, USA).

2.6.3. ALP assay alkaline phosphatase activity quantification

The retention of osteoblastic phenotype at days 8, 14, 28 and 56 was evaluated by measuring alkaline phosphatase activity using a colorimetric method, which is based on the conversion of *p*-nitrophenyl phosphate into *p*-nitrophenol in the presence of the alkaline phosphatase. The hFOB seeded scaffold samples were removed from the incubator at different culturing periods. These samples were first washed with PBS and then placed into 1 mL 0.1% Triton X solution to be subsequently stored at −80 °C. Following three freeze–thaw cycles, a volume of 20 μl of supernatant was taken from the samples and added into 100 μl of 1 mg/mL *p*-nitrophenyl phosphate substrate (Sigma) solution in diethanolamine substrate buffer (Pierce) at room temperature for 30 min. Reaction was stopped by adding 50 μl of 2 M NaOH solution and waiting for 5 min. The production of *p*-nitrophenol was determined by measuring the absorbance with a SYNERGY HT plate reader (KC4, BIO-TEK, USA). The molar concentration of alkaline phosphatase of each sample was determined using a calibration curve and the results were normalized by the protein concentration of each sample, which was measured using Bradford protein assay as explained in Section 2.3. The results for alkaline phosphatase activity assay were reported as nmol alkaline phosphatase/mg protein.

2.6.4. Cell morphology and penetration depth by SEM, confocal laser microscopy and histology

Some of the hFOB cultured samples were first washed with PBS followed by being fixed with 4% paraformaldehyde (mass fraction) in PBS and then were kept at 4 °C (for at least 12 h). Fixed samples were washed with PBS again, followed by staining using phalloidin (Invitrogen) for confocal microscopy. A Nikon E1000 confocal laser microscope was used to image cells at different locations of the scaffold to elucidate cell penetration patterns. Histological evaluation of scaffolds was also carried out after fixing the samples in buffered 4% formaldehyde solution, followed by dehydration using a series of graded ethanol solutions (starting with 70% and increasing to 100% ethanol at 10% increments) and embedding in glycol methacrylate. Thin cross sections (5 μm) were obtained from embedded samples and they were stained with hematoxyline and eosin (H&E) and toluidine blue (TB) to examine the cell distribution and morphology in the constructs. The stained sections were analyzed using Olympus BX-50 Polarizing Microscope. Some of the construct samples were prepared for SEM, EDX and EDS analyses upon washing with deionized water after fixation, dehydration in graded ethanol changes and drying at room temperature.

2.7. Data analysis

At least three samples per condition were used for all experiments. All data are reported in terms of ±95% confidence intervals, determined according to Student's *t* distribution.

3. Results and discussion

3.1. Structural, morphological and compressive properties of the scaffolds

The designations and the details of the processing conditions for the scaffolds of this study are provided in Table 1. The mean porosity values of the scaffolds are in the 69–80% range for wet extruded and 69–77% for melt extruded, with the scaffolds designated as W3 exhibiting the highest porosity and W4 exhibiting the lowest (Table 1). These porosity values are significantly greater than the porosity values that are achieved by some other methods including sintering of microspheres (29–42% porosity) [22]. The bulk crystallinity values of the scaffolds determined using DSC are also shown in Table 1. The ranges of crystallinity values are 43–50% for the wet extruded samples and 44–48% for the melt extruded PCL samples.

Fig. 2a and b shows the SEM micrographs of melt extruded sample (with designation of M3) that were extruded at 100 °C (Table 1), obtained upon the cryofracture of the specimen in the transverse to flow direction (Fig. 2a and b). These micrographs are characteristic of the overall interconnectivity and surface topographies of all three types of melt extruded scaffold samples. SEM micrographs revealed that melt extruded scaffolds exhibit two different levels of pore sizes; macropores generated by the dissolution of the salt porogens that are in the 10–200 μm size range and nano and micropores in the 100–1000 nm range (presumably generated by the dissolution of the PEO). The ability to generate multi-scaled porosities can be considered to be an important structuring ability since the surface to volume ratio of such scaffolds would change significantly, especially upon the formation of nanopores. Such a significant increase of the surface to volume ratio of the scaffold would affect the release rate of the protein and possibly the adhesion and proliferation rate of cells that are cultured on such scaffolds.

Fig. 2c and d provides the typical SEM micrographs of wet extruded scaffold samples (only micrographs from W3 are included here since the micrographs obtained from W1, W2 and W4 reveal similar structures and connectivity). Micrographs of the wet extruded scaffolds (Fig. 2c and d) reveal macropores in the 10–600 μm range, which appear to be well interconnected. The surface topographies of wet extruded scaffolds differ in one significant aspect from those that are melt extruded upon the blending of two resins, PEO and PCL (Fig. 3a, b). As shown clearly in Fig. 3a and b, no nano or micropores exist at the walls of the wet extruded samples as observed with the melt extruded scaffolds from the PEO/PCL blends (shown in Fig. 2a and b). Furthermore, the wet extruded

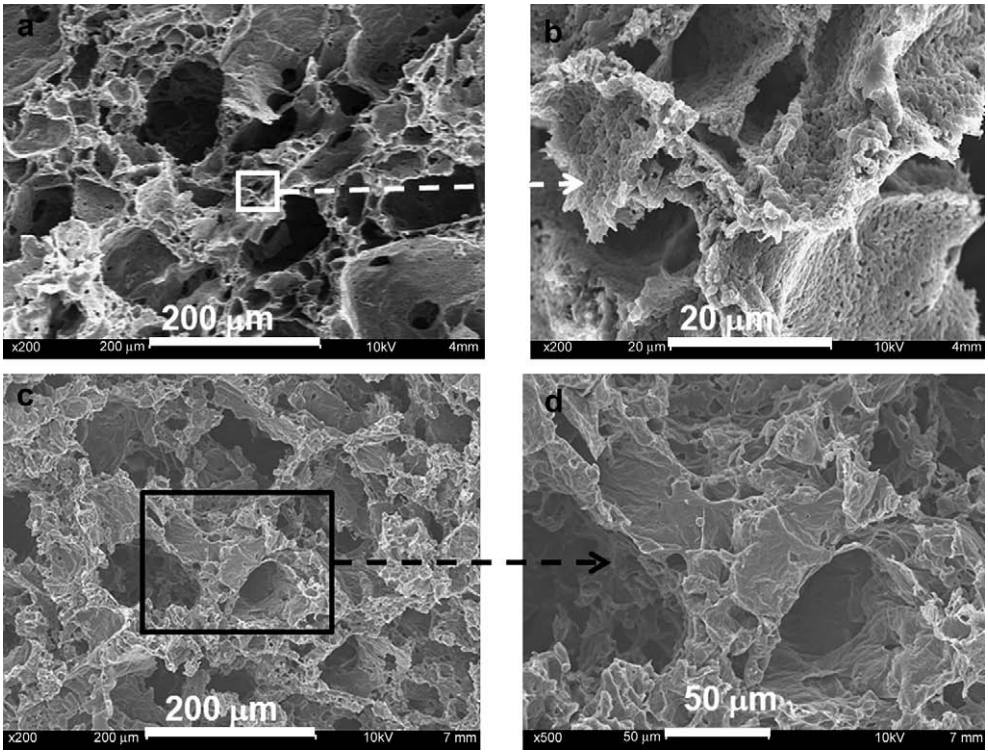

Fig. 2. SEM micrographs of cryo-fractured melt extruded M3 type scaffolds at low (a) and high (b) magnifications revealing two different levels of pore sizes; macropores generated by the dissolution of the salt porogens and nano and micropores generated by the dissolution of the PEO. SEM micrographs of cryo-fractured wet extruded W3 type scaffolds at low (c) and high (d) magnifications revealing well-interconnected macropores.

scaffolds appear to exhibit grooves with depths of 100–500 nm and groove widths in the 500 nm to 1 μm range (Fig. 3b). The development of such grooves can be an important structuring effect, since it is known that the cells can orient along the length direction of the grooves during their proliferation [35,36].

The porosity is determined to be uniform along the extrusion direction throughout both the wet and melt extruded scaffolds. Such uniformity is realized through the dispersion capability of the twin screw extruder. Furthermore, the availability of homogeneously distributed, highly concentrated salt particles prior to leaching should be instrumental in the prevention of the collapse of the wet polymer upon extrusion, thus enabling the fabrication of scaffolds with relatively high porosity and structural integrity. The formation of the nanopores in the wet extruded scaffolds is an interesting structuring effect that could have also been obtained with the freeze drying process but the typical temperatures involved in freeze drying would have been detrimental to protein stability [37,38].

The compressive properties are first and foremost affected by the porosity of the scaffolds (Table 1). The compressive modulus and the compressive yield stress of the scaffold specimens decreased with increasing porosity (Table 1), similar to the findings of the earlier studies [39,40]. Increasing the porosity from 69% (W4) to 80% (W3) resulted in decreases of the elastic modulus (slope of the nominal compressive stress versus compressive strain in the linear region), E, from 81 kPa to 30 kPa and compressive yield strength, σ, from 748 kPa to 250 kPa. The compressive properties can be manipulated further by changing the polymer molecular weight as well as the pore size and porosity distributions [39].

3.2. Protein encapsulation efficiency

The protein encapsulation efficiency values of scaffolds fabricated by wet and melt extrusion methods with different porosity values are reported in Table 1. The results indicate that protein encapsulation efficiency decreases with increasing porosity for both wet and melt extruded samples. BSA encapsulation efficiency value decreases from 59% (W4) to 29% (W3) when porosity increases from 69% (W4) to 80% (W3) for wet extruded scaffolds. A similar trend was also observed for melt extruded scaffolds. Encapsulation efficiency values decrease from 38% (M1) to 28% (M3) with increasing porosity from 69% (M1) to 77% (M3). These findings are consistent with the higher surface to volume ratio of the scaffolds that exhibit greater porosity leading to higher rates of protein loss during the salt leaching process.

The fabrication method, i.e., wet versus melt extrusion, has an effect on encapsulation efficiency at constant porosity. Wet and melt extruded samples with similar porosity values exhibit differing encapsulation efficiency values. This is evident, for example, from the comparison of the encapsulation efficiency values of sample W4 and M2 (both exhibit 69% porosity) given in Table 1. Wet extruded sample W4 has an encapsulation efficiency of 59% whereas the melt extruded sample has 38% encapsulation efficiency. In the melt extrusion process used in this study, BSA-coated PCL powder was pre-blended with PEO powder and it is possible that during the melting and mixing process BSA could be encapsulated in both PCL and PEO phases. This should lead to a higher amount of BSA loss due to the dissolution removal of PEO over and above the BSA loss from the PCL surfaces that are in contact with water. The encapsulation efficiency may be improved further by feeding BSA-coated PCL powder as a first feed stream into the extruder and the melting and mixing of the PCL/BSA phases in the extruder prior to the feeding of the PEO and the salt as the second and third feed streams.

Overall the BSA encapsulation efficiency values reported here are in line with other protein encapsulation processes including the use of sintered microspheres [22]. For example, Luciani et al. have

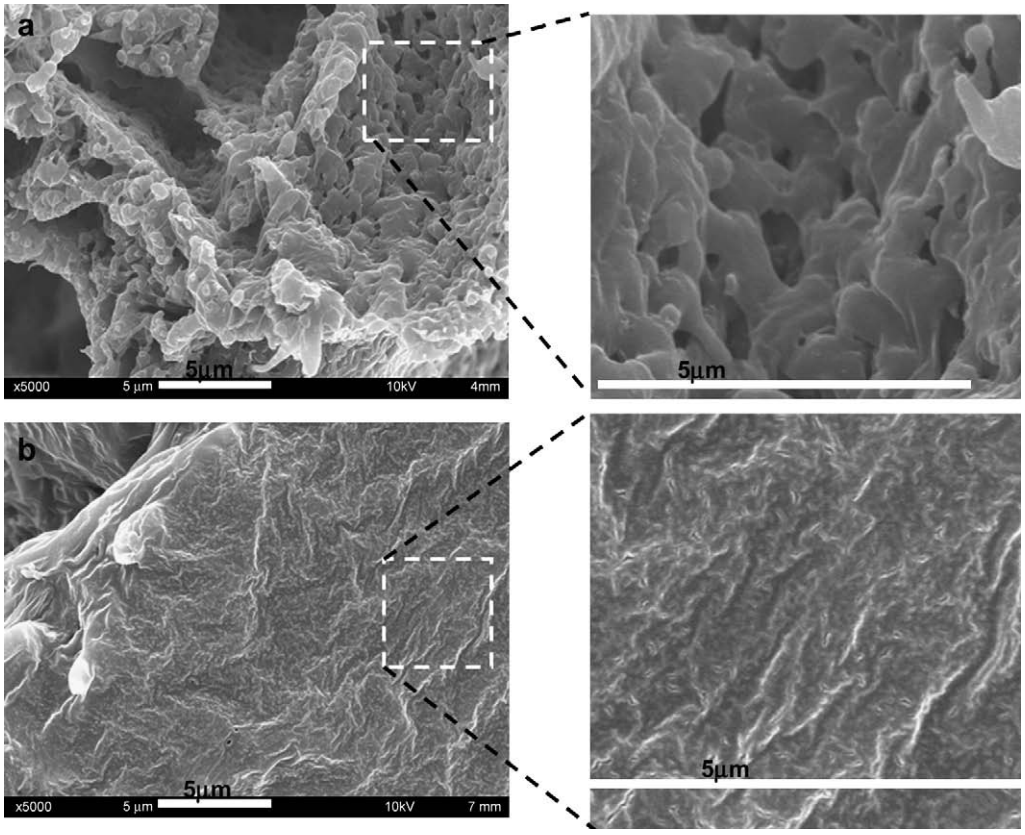

Fig. 3. Pore morphology and surface topography of melt extruded M3 (a) and wet extruded W3 (b) type scaffolds at different magnifications.

reported that the encapsulation efficiency values in BSA loaded PCL microspheres are in the range 29.1–62.9% [22].

3.3. In vitro BSA release study

Fig. 4a shows the cumulative release percentage of total encapsulated BSA and Fig. 4b shows the cumulative release rate of BSA (μg BSA/mg scaffold) from wet and melt extruded scaffolds with different porosity values. The scaffolds exhibit an initial burst effect followed by a slow release rate profile. The differences in the cumulative percent release of BSA exhibited by the different scaffolds are obviously related to the amounts of BSA that are released into the water phase during the porosity-generating dissolution of salt and PEO in water. Fig. 4 shows that the cumulative released BSA amount does not exceed over 15% of the total BSA quantity encapsulated in the W4 scaffold during the burst period. This value is 8% for M1, 10% for M2 and M3 and 3% for W1 scaffolds. Thus, the additional release of the protein from the polymer that it is encapsulated into would largely depend on the degradation rate of the biodegradable polymer.

The degradation rate of the polymer is typically a function of polymer properties such as polymer composition, molecular weight and crystallinity [41]. The release results reported in Fig. 4 suggest that the initial burst of the protein can be manipulated by altering the fabrication method and the resulting porosity distribution of the scaffold. Furthermore, a significant proportion of the protein encapsulated in the polymer is retained after the 40 days duration of the in vitro study (86–97%) to be released in line with the relatively slow degradation rate of PCL over a prolonged time scale. Fig. 4b shows the cumulative release rate of BSA (μg BSA per mg of scaffold versus time). The release rate of the protein can be tailored simply by changing the initial loading amount of the protein and the porosity and pore morphology of the scaffold.

3.4. Stability of BSA secondary structure

The encapsulation process using melt and wet extrusion processes can exhibit potentially harsh conditions, possibly leading to the denaturing of the encapsulated or the structure modification of the encapsulated proteins. Some important factors to consider include the presence of organic solvents during wet extrusion process and the relatively high shear stresses, increased residence times and elevated temperatures experienced by the biomaterial during the melt extrusion process. In order to evaluate the rate of irreversible protein structure modification, a series of far-UV circular dichroism measurements were performed on the native BSA and on the BSA released from extruded scaffolds.

The characteristic far-UV spectra of native BSA and release samples from extruded scaffolds are shown in Fig. 5. All samples have minima at 209 and 222 nm indicative of the prevailing predominantly α-helical secondary structure (Fig. 5). Far-UV spectra of wet extruded sample are not altered significantly compared to native BSA indicating that secondary structure is preserved upon protein encapsulation with wet extrusion process. This should be related to the relatively low shearing stresses (1.14 kPa maximum at the wall of the die), low temperature (<25 °C) and the absence of an aqueous/organic mixture in the process with restricted conformational mobility [42] in the wet extrusion process.

On the other hand, the intensities of the two minima of melt extruded samples were smaller than those of the native BSA, indicating a certain level of decrease in the α-helix content of the released BSA from melt extruded scaffolds. CDPro software was

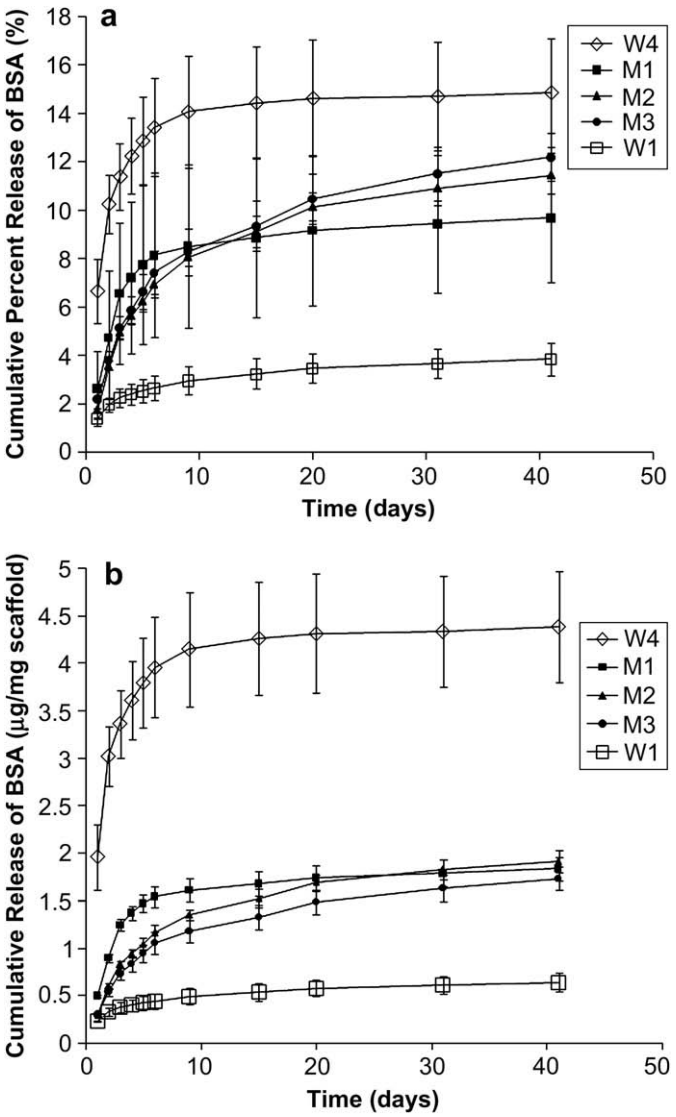

Fig. 4. Cumulative release percentage (%) of total encapsulated BSA (a) and cumulative release rate of BSA (µg BSA/mg scaffold) from different types of hot melt extruded (M1, M2 and M3) and wet extruded (W1 and W4) scaffolds.

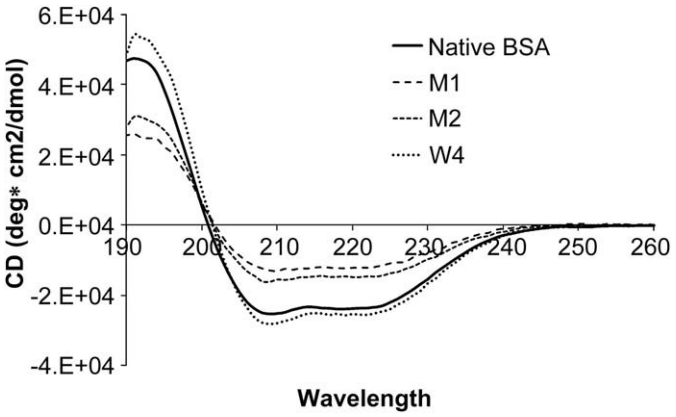

Fig. 5. Far-UV circular dichroism (CD) spectrum of released BSA from hot melt extruded M1, M2 and wet extruded W4 types of scaffolds compared to unprocessed native BSA solution in PBS buffer after background correction. All samples have minima at 209 and 222 nm indicative of the prevailing predominantly α-helical secondary structure.

Table 2
Percent of secondary structure components of native and released BSA.

Sample designation	Native BSA	M1	M2	W4
α-Helix	70.2 ± 1.7	39.7 ± 0.5	49.2 ± 1.7	74.2 ± 2.4
β-Sheet	3.6 ± 2.6	15.7 ± 1.1	10.5 ± 0.4	1.9 ± 3.3
Turns	9.8 ± 1.5	16.5 ± 0.5	15.5 ± 1.8	6.5 ± 1.9
Un-ordered	17.6 ± 2.7	28.2 ± 2	24.9 ± 0.3	15 ± 4.6

used to calculate the percentage of α-helix and β-sheets of the protein. These results are shown in Table 2. The data show that native BSA contains 70.2 ± 1.7% α-helixes and 3.6 ± 2.6% of β-sheets. Wet extruded sample W4 contains 74.2 ± 2.4% of α-helixes, melt extruded samples M1 and M2 contain 39.7 ± 0.5% and 49.2 ± 1.7% α-helixes, respectively.

The conformational change of the melt extruded samples should be associated with the elevated temperatures as well as elevated stress magnitudes of the melt extrusion process. When the temperature increases above the glass transition temperature of the protein significant denaturing of the protein occurs [43]. In our melt processing experiment the melt temperatures were in the 80–100 °C range, and thus the temperature increased above the glass transition temperature of BSA, which is 60 °C.

The other factor that can play a role is the level of stress that the protein is exposed to during the processing operation. The processing temperature of M2 is higher than the processing temperature of M1 but Fig. 5 suggests that the secondary structure of M2 is changed less than the secondary structure of M1. The shear viscosity of the mixture inside the extruder would increase when the processing temperature decreases at constant flow rate and screw speed and as a result of this increased viscosity, the stress magnitudes (summation of shearing and extensional velocity gradients) exerted onto BSA would also increase. The typical shearing stress maxima observed in our experiments at the die during melt extrusion is 140 kPa at 80 and 91 kPa at 100 °C. These results suggest that the higher shear stress values associated with processing at the lower 80 °C temperature has a more pronounced effect on the secondary structure of the protein compared to the effect of 100 °C processing temperature at lower shear stresses, consistent with the findings of Ref. [44].

3.5. Cell–scaffold interactions

Human fetal osteoblast, hFOB, cells attached to the scaffold surfaces producing three dimensional, porous hFOB cell constructs for both wet and melt extruded scaffolds. The cell viability and proliferation rates were investigated by measuring the metabolic activity of the hFOB cells (MTS assay) as a function of time at 37 °C. The results for the scaffold types W1, W3 and M3 in comparison to standard tissue culture plates used as control are given in Fig. 6a. The metabolic activity of hFOB cells increased with time, indicating that the hFOB cells were viable and proliferating during the 56 days duration of the study for all three types of scaffolds. The significant differences between the control and the scaffold samples are associated with the initial lower seeding density of cells on the scaffolds versus the seeding density on the controls (in culturing of cells on the scaffolds only 30% were found to reside on the scaffold surface whereas 70% were attached to the walls of the culturing plates).

Fig. 6a shows that hFOB proliferation rate leveled off and declined in all the tissue constructs studied and on reference tissue culture plate after 28 days in culture, with a significant change in cell numbers between days 28 and 56. This can be explained by the reciprocal and functionally coupled relationship between proliferation and differentiation rates [45]. It is reported that the synthesis of a bone extracellular matrix and its accumulation and maturation

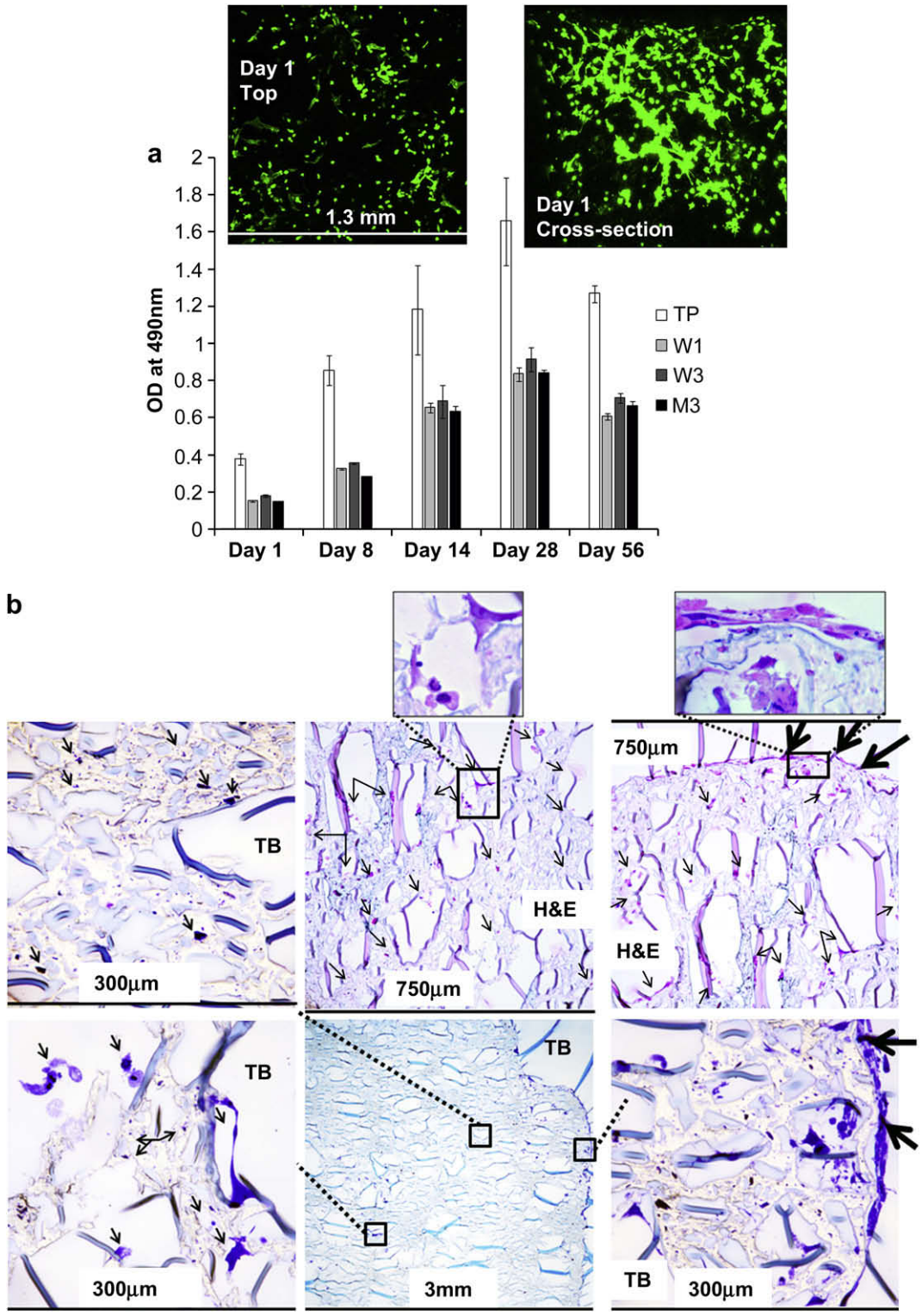

Fig. 6. Optical density, OD, obtained from MTS assay, versus culture time of W1, W3 and M3 scaffolds (a). Insets show the confocal laser microscopy images of phalloidin stained W3 scaffold after 1 day of incubation. Green color is indicative of the actin filaments of hFOB cells (a). Optical microscopy images of toluidine blue (TB) and H&E stained W3 scaffold following 56 days of incubation. Small arrows are indicative of the ECM matrix deposition of W3 type of scaffold (blue color stained regions for TB stained sections and pink and purple color stained regions for H&E stained sections). Large arrows are indicative of the formation of cell layers on top surface of the scaffold (on which cells were seeded). The image locations are indicated on each micrograph via broken lines (b).

lead to osteoblasts being trapped and embedded in the mineralizing matrix and consequently the shutdown of the proliferation [45], which should lead to the abrupt change in the proliferation rate observed at 28 days.

Insets of Fig. 6a show the confocal laser microscopy images of phalloidin stained actin filaments of attached hFOB cells on the top surface and throughout the cross-section of wet extruded W3 type scaffold after 24 h of incubation. Fig. 6b shows the optical

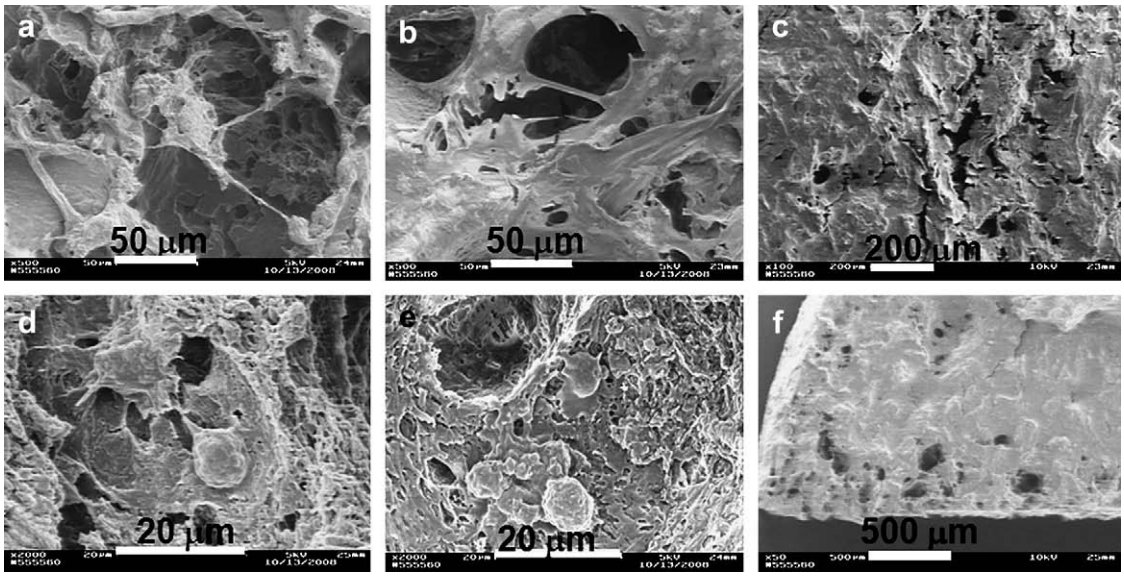

Fig. 7. SEM micrographs of cell attachment of hFOB cells on W3 and M3 scaffolds after 24 h of incubation (a and d). The surfaces of the scaffolds were partially covered with hFOB cells after 8 days of incubation (b and e) and fully covered with hFOB cells after 14 days of incubation (c and f).

microscopy images of H&E stained and TB stained W3 type scaffold sections after 56 days of incubation. After 56 days of culturing, a noticeable amount of new ECM was observed in the inter-pore space across the entire scaffold cross-section. Fig. 6a and b confirms that the interconnectivity of the porous structure of the scaffolds has indeed allowed the cells to proliferate and penetrate into the volume of the entire scaffold.

Scanning electron micrographs of Fig. 7 show the typical morphology of the osteoblast cells attached to the pore walls of the scaffolds after 24 h, 8 days and 14 days. There seems to be a difference between the morphology of the initially attached cells on wet (W3) and melt (M3) extruded scaffolds after 24 h and 8 days (Fig. 7a, b, d and e). Fig. 7 indicates that the hFOB cells have bridged over and covered the pore cavities by forming a flat cell layer on wet extruded W3 type scaffolds after 8 days in culture (Fig. 7b) but not on melt extruded M3 type scaffolds (Fig. 7e). Fig. 7c and f further shows the formation of a confluent cell layer on cell seeding surfaces of both melt (M3) and wet (W3) extruded scaffolds covering the entire pore surfaces after 14 days in culture. Other studies, which were carried out on 3D porous surfaces reported that the hFOB cells form a well spread flat cell layer after 24 h [46]. Coombes et al. observed that surface texture has an effect on cell attachment and proliferation, for example, hFOB cell attachment and growth were enhanced on microporous PCL surfaces in comparison to those observed upon using smooth PCL films [46]. This was explained on the basis of the competitive and selective adsorption of cell adhesion molecules, such as fibronectin, due to increased surface area of microporous surfaces and the positive effect of surface topography on mechanical stresses experienced by the cytoskeleton [47,48].

Ideally, the height of the protrusions should be small and the spacing between the protrusions should be large enough to enable the clustering of integrins, which is a requirement for the formation of mature and stable focal adhesions [49]. The typical surface topographies of our scaffold surfaces (Fig. 3) indicate that the scale of protrusions on the surface is in the 500–1000 nm range. Such texture should not prevent cell cytoplasm to expand well in all directions and is expected to trigger the expression of typical bone differentiation markers [50].

Alizarin Red Ca^{2+} quantification assay results are given in Fig. 8 and suggest that Ca^{2+} deposition increased upon 56 days of culturing. Tissue constructs obtained from the wet extruded W3 type scaffolds (with the highest porosity of 80%) exhibited the highest rate of Ca^{2+} deposition, whereas the tissue constructs obtained from the melt extruded M3 type scaffolds exhibited the lowest rate. Insets of Fig. 8 show the Ca^{2+} deposits, as revealed by Alizarin Red staining, on type M1 scaffolds after 14 days (designated as a) and on type W3 type scaffold surfaces after 56 days culturing (designated as b). Alizarin Red stain shows the bone nodule formation and mineralization both at the surfaces and within the bulk of 2.5 mm thick tissue constructs (Fig. 8b). The deposition of the Ca was further investigated using EDX mapping. Fig. 9 shows a typical SEM micrograph of the cell layer formed on W1 type scaffolds after 28 days of culturing and its corresponding EDX mapping and spectrum. EDX results indicate the existence of calcium and phosphate deposition on the cell layer.

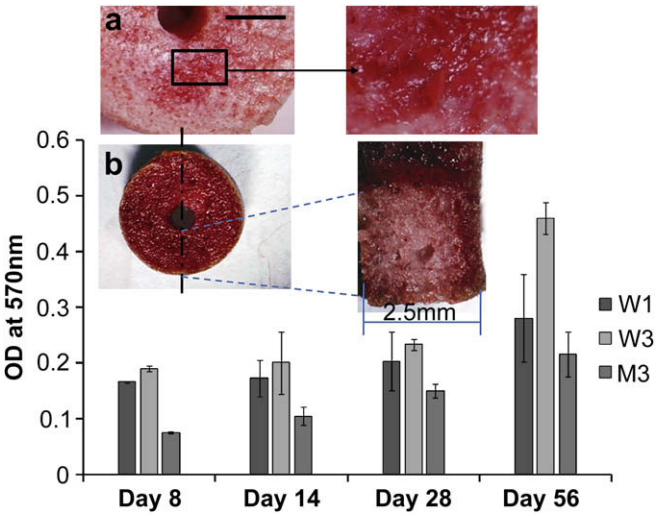

Fig. 8. Optical density, OD, obtained from Alizarin Red assay for Ca^{2+} deposition. Inset shows the stereo-optical microscopy images of hFOB cells on M3 type scaffold after ALZ staining upon 14 days of culture (a) (scale bar represents 1 mm) and on W3 scaffold (8 mm outer diameter, 1.5 mm inner diameter and 2.5 mm thickness) after 56 days of culture (b). Orange/red color represents mineralized extracellular matrix formation.

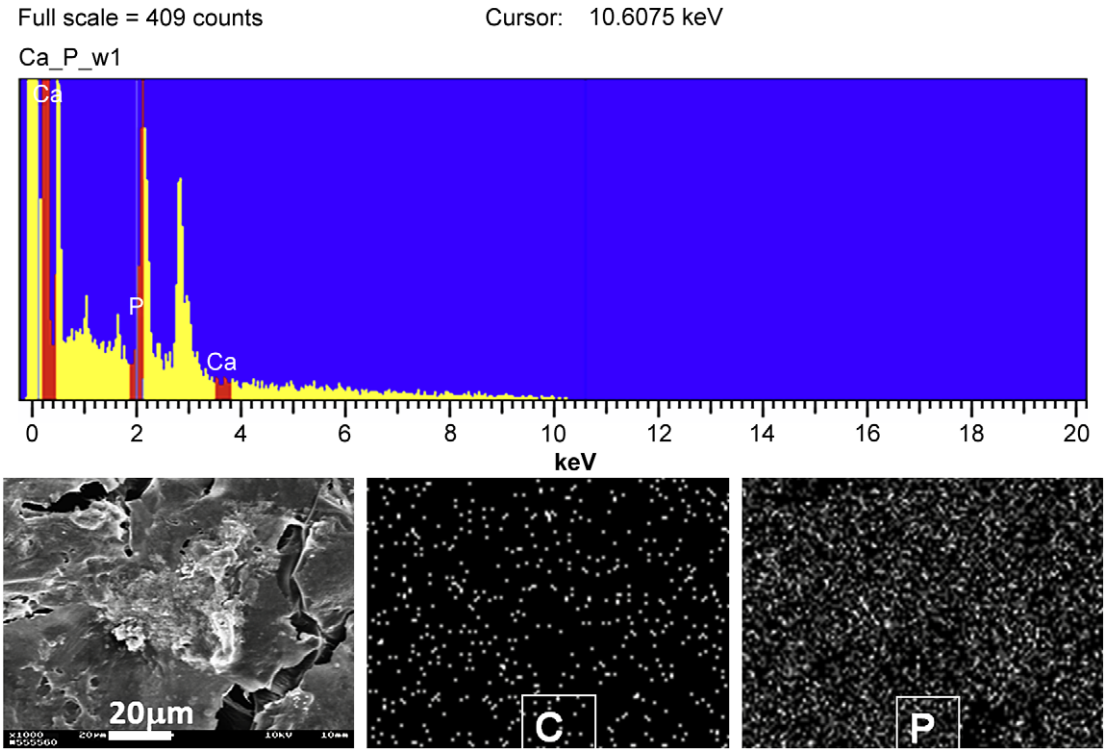

Fig. 9. SEM micrograph of hFOB cell layers on W1 scaffold after 28 day culturing and its corresponding EDX mapping and spectrum showing calcium and phosphate deposition.

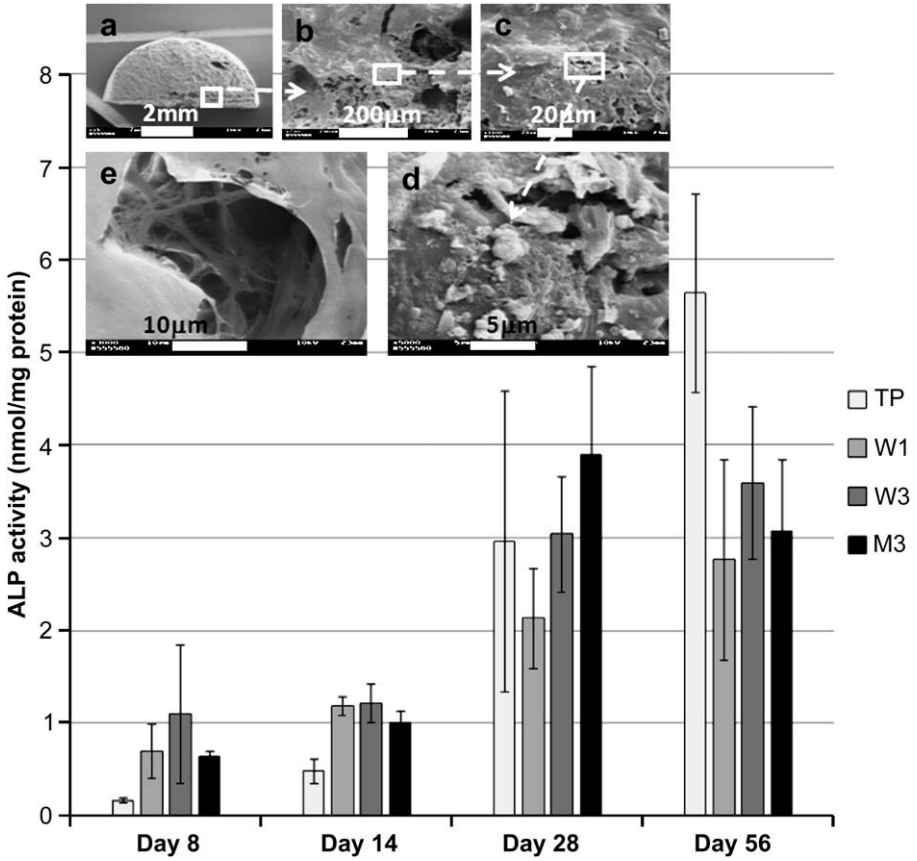

Fig. 10. ALP activity (nmol alkaline phosphatase/mg protein) of tissue cultures obtained with W1, W3 and M3 scaffolds compared to cells on standard tissue culture plates (TP) at 8, 14, 28 and 56 days of culturing. Insets show the confluent hFOB cell layers formed after 28 days culturing on wet extruded W3 scaffolds (a–e) Ca^{2+} deposition (d) and formation of collagen bundles (e).

The phenotypic expressions of cells cultured on wet and melt extruded scaffolds were evaluated by colorimetric analysis for alkaline phosphatase activity at days 8, 14, 28 and 56. The expression of alkaline phosphatase, ALPase, and thus the expression of the bone cell phenotype, increased significantly at day 28 (Fig. 10) followed by a leveling off. These results are in line with previous studies focusing on human bone marrow stem cells, cultured in the same differentiation media used in this study [45]. The typical formation of collagen bundles and Ca deposition on surfaces of W3 type scaffolds, further suggesting osteoblastic differentiation, are shown in the insets of Fig. 10.

4. Conclusions

The capabilities of a recently developed twin screw extrusion spiral winding process, TSESW, for generating protein-encapsulated tissue engineering scaffolds were demonstrated in conjunction with fabrication of porous polycaprolactone scaffolds incorporated with BSA. Both wet and hot melt extrusion methods were applied. Processing conditions and porosity of the scaffolds were changed to enable the investigation of the effects of parameters such as porosity, pore size, existence of organic solvents, temperature and shear stress levels on the secondary structure of BSA. Using hFOB cells it was demonstrated that the resulting functionalized multilayered tubular scaffolds are non-cytotoxic with favorable cell adhesion, penetration and differentiation rates associated with the tailored distributions of porosity and chemical composition. This new technology base for the fabrication of tissue engineering scaffolds offers the following in overcoming some of the current limitations of tissue engineering:

1. Using TSESW the tissue engineering scaffolds can be incorporated with systematic distributions in composition and porosity in a reproducible and industrially-relevant i.e., scalable mode.
2. The distributions of the composition and porosity in the scaffolds can be tailored, i.e., functionally graded, in a three dimensional manner with a wide latitude in compositions and porosities that can be achieved systematically.
3. The functionally-graded scaffolds can be further incorporated with various mediators and growth factors to furnish three dimensional mediator/protein distributions to allow three dimensional differentiation.

Thus, the proposed methodology is a step that is in the right direction for tissue engineering, i.e., in the development of on-demand tissue constructs. Tissue engineering is based first on the definition and specification of what type of cells, angiogenesis and extracellular matrix distributions need to be generated in the tissues targeted to be repaired/replaced, followed by the corresponding specifications of what are required in terms of the three dimensional distributions of properties and compositions of the tissue engineering scaffolds. TSESW will provide additional versatility to generate the desired scaffold structural and composition distributions.

Acknowledgements

We are grateful to Merck Research Laboratories for their partial financial support in terms of a Merck Research Laboratories Fellowship in Chemistry, Pharmaceutical Science, Material Science, and Engineering to Ms. Seher Ozkan. We thank Material Processing & Research Inc. of Hackensack, NJ for making their MPR 7.5 mm twin screw extrusion platform available for our investigation. We thank Professor Frank Fisher of Stevens for his help with the characterization of compressive properties and Dr. Roxana Ionescu, Ms. Shiyi Wang, Mr. Stephen Wahn, Ms. Lixia Cai and Dr. Chad David Brown of Merck for their guidance and input for circular dichroism, granulation and controlled release. We are also thankful to Dr. Markus F. Meyenhofer of University of Medicine and Dentistry of New Jersey for his help in histological analyses and Chandra M. Valmikinathan of Stevens for his help in confocal laser microscopy.

Appendix

Figures with essential colour discrimination. Fig. 8 in this article may be difficult to interpret in black and white. The full colour images can be found in the on-line version, at doi:10.1016/j.biomaterials.2009.04.050.

References

[1] Langer R, Vacanti JP. Tissue engineering. Science 1993;260:920–6.
[2] Mikos AG, Herring SW, Ochareon P, Elisseeff J, Lu HH, Kandel R, et al. Engineering complex tissues. Tissue Eng 2006;12(12):3307–39.
[3] Causa F, Netti PA, Ambrosio L. A multi-functional scaffold for tissue regeneration: the need to engineer a tissue analogue. Biomaterials 2007;28(34):5093–9.
[4] Sands RW, Mooney DJ. Polymers to direct cell fate by controlling the microenvironment. Curr Opin Biotechnol 2007;18(5):448–53.
[5] Lutolf MP, Hubbell JA. Synthetic biomaterials as instructive extracellular microenvironments for morphogenesis in tissue engineering. Nat Biotechnol 2005;23(1):47–55.
[6] Erisken C, Kalyon DM, Wang H. Functionally graded electrospun polycaprolactone and β-tricalcium phosphate nanocomposites for tissue engineering applications. Biomaterials 2008;29:4065–73.
[7] Kaplan DL, Moon RT, Vunjak-Novakovic G. It takes a village to grow a tissue. Nat Biotechnol 2005;23(10):1237–9.
[8] Shea LD, Smiley E, Bonadio J, Mooney DJ. Nat Biotechnol 1999;17:551–4.
[9] Benoit DSW, Schwartz MP, Durney AR, Anseth KS. Small functional groups for controlled differentiation of hydrogel-encapsulated human mesenchymal stem cells. Nat Mater 2008;7:816–23.
[10] Rives CB, des Rieux A, Zelivyanskaya M, Stock SR, Lowe Jr WL, Shea LD. Layered PLG scaffolds for in vivo plasmid delivery. Biomaterials 2009;30(3):394–401.
[11] Fu K, Klibanov AM, Langer R. Protein stability in controlled release systems. Nat Biotechnol 2000;18:24–5.
[12] Archer R, Williams DJ. Why tissue engineering needs process engineering. Nat Biotechnol 2005;23(11):1353–5.
[13] Whang K, Goldstick TK, Healy KE. A biodegradable polymer scaffold for delivery of osteotropic factors. Biomaterials 2000;21(24):2545–51.
[14] Richardson TP, Peters MC, Ennett AB, Mooney DJ. Polymeric system for dual growth factor delivery. Nat Biotechnol 2001;19(11):1029–34.
[15] Carrasquillo KG, Stanley AM, Aponte-Carro JC, De Jésus P, Costantino HR, Bosques CJ, et al. Non-aqueous encapsulation of excipient-stabilized spray-freeze dried BSA into poly(lactide-co-glycolide) microspheres results in release of native protein. J Control Release 2001;76(3):199–208.
[16] Chang HI, Williamson MR, Perrie Y, Coombes AG. Precipitation casting of drug-loaded microporous PCL matrices: incorporation of progesterone by co-dissolution. J Control Release 2005;106(3):263–72.
[17] Yang Y, De Laporte L, Rives CB, Jang JH, Lin WC, Shull KR, et al. Neurotrophin releasing single and multiple lumen nerve conduits. J Control Release 2005;104(3):433–46.
[18] Rai B, Teoh SH, Hutmacher DW, Cao T, Ho KH. Novel PCL-based honeycomb scaffolds as drug delivery systems for rhBMP-2. Biomaterials 2005;26(17):3739–48.
[19] Sohier J, Vlugt TJ, Cabrol N, Van Blitterswijk C, de Groot K, Bezemer JM. Dual release of proteins from porous polymeric scaffolds. J Control Release 2006;111(1–2):95–106.
[20] Lee M, Chen TT, Iruela-Arispe ML, Wu BM, Dunn JC. Modulation of protein delivery from modular polymer scaffolds. Biomaterials 2007;28(10):1862–70.
[21] Jaklenec A, Wan E, Murray ME, Mathiowitz E. Novel scaffolds fabricated from protein-loaded microspheres for tissue engineering. Biomaterials 2008;29(2):185–92.
[22] Luciani A, Coccoli V, Orsi S, Ambrosio L, Netti PA. PCL microspheres based functional scaffolds by bottom-up approach with predefined microstructural properties and release profiles. Biomaterials 2008;29(36):4800–7.
[23] Ginty PJ, Barry JJ, White LJ, Howdle SM, Shakesheff KM. Controlling protein release from scaffolds using polymer blends and composites. Eur J Pharm Biopharm 2008;68(1):82–9.
[24] Wang J, Cheung MK, Mi Y. Miscibility and morphology in crystalline/amorphous blends of poly(caprolactone)/poly(4-vinylphenol) as studied by DSC, FTIR and ^{13}C solid state NMR. Polymer 2002;43:1357–64.

[25] Tice TR, Gilley RM, Eldridge JH, Staas JK. Composition for delivering bioactive agents for immune response and its preparation. US Patent No. 6024983; 2000.
[26] Yu X, Botchwey EA, Levine EM, Pollack SR, Laurencin CT. Bioreactor-based bone tissue engineering: the influence of dynamic flow on osteoblast phenotypic expression and matrix mineralization. Proc Natl Acad Sci U S A 2004;101(31):11203–8.
[27] Popat KC, Leary Swan EE, Mukhatyar V, Chatvanichkul KI, Mor GK, Grimes CA, et al. Influence of nanoporous alumina membranes on long-term osteoblast response. Biomaterials 2005;26(22):4516–22.
[28] Ignatius A, Blessing H, Liedert A, Schmidt C, Neidlinger-Wilke C, Kaspar D, et al. Tissue engineering of bone: effects of mechanical strain on osteoblastic cells in type I collagen matrices. Biomaterials 2005;26(3):311–8.
[29] Jones JR, Tsigkou O, Coates EE, Stevens MM, Polak JM, Hench LL. Extracellular matrix formation and mineralization on a phosphate-free porous bioactive glass scaffold using primary human osteoblast (HOB) cells. Biomaterials 2007;28(9):1653–63.
[30] Skelton KL, Glenn JV, Clarke SA, Georgiou G, Valappil SP, Knowles JC, et al. Effect of ternary phosphate-based glass compositions on osteoblast and osteoblast-like proliferation, differentiation and death in vitro. Acta Biomater 2007;3(4):563–72.
[31] Cuddihy MJ, Kotov NA. Poly(lactic-co-glycolic acid) bone scaffolds with inverted colloidal crystal geometry. Tissue Eng Part A 2008;14(9):1639–49.
[32] Subramaniam M, Jalal SM, Rickard DJ, Harris SA, Bolander ME, Spelsberg TC. Further characterization of human fetal osteoblastic hFOB 1.19 and hFOB/ER alpha cells: bone formation in vivo and karyotype analysis using multicolor fluorescent in situ hybridization. J Cell Biochem 2002;87(1):9–15.
[33] Montjovent MO, Burri N, Mark S, Federici E, Scaletta C, Zambelli PY, et al. Fetal bone cells for tissue engineering. Bone 2004;35(6):1323–33.
[34] Botchwey EA, Pollack SR, Levine EM, Laurencin CT. Bone tissue engineering in a rotating bioreactor using a microcarrier matrix system. J Biomed Mater Res 2001;55(2):242–53.
[35] Matsuzaka K, Yoshinari M, Shimono M, Inoue T. Effects of multigrooved surfaces on osteoblast-like cells in vitro: scanning electron microscopic observation and mRNA expression of osteopontin and osteocalcin. J Biomed Mater Res A 2004;68:227–34.
[36] Degirmenbasi N, Ozkan S, Kalyon DM, Yu X. Surface patterning of poly(ι-lactide) upon melt processing: in vitro culturing of fibroblasts and osteoblasts on surfaces ranging from highly crystalline with spherulitic protrusions to amorphous with nanoscale indentations. J Biomed Mater Res A 2008;88A(1):94–104.
[37] Zhang R, Ma PX. Poly(alpha-hydroxyl acids)/hydroxyapatite porous composites for bone-tissue engineering. I. Preparation and morphology. J Biomed Mater Res 1999;44(4):446–55.
[38] Wang W. Instability, stabilization and formulation of liquid protein pharmaceuticals. Int J Pharm 1999;185:129–88.
[39] Karageorgiou V, Kaplan D. Porosity of 3D biomaterial scaffolds and osteogenesis. Biomaterials 2005;26(27):5474–91.
[40] Thomson RC, Yaszemski MJ, Powers JM, Mikos AG. Fabrication of biodegradable polymer scaffolds to engineer trabecular bone. J Biomater Sci Polym Ed 1996;7(1):23–38.
[41] Anderson JM, Shive MS. Biodegradation and biocompatibility of PLA and PLGA microspheres. Adv Drug Deliv Rev 1997;28(1):5–24.
[42] Griebenov K, Klibanov AM. On protein denaturation in aqueous–organic mixtures but not in pure organic solvents. J Am Chem Soc 1996;118:11695–700.
[43] Lai MC, Topp EM. Solid state chemical stability of proteins and peptides. J Pharm Sci 1999;88:489–500.
[44] Sah H. Protein instability toward organic solvent/water emulsification: implication for protein microencapsulation into microspheres. PDA J Pharm Sci Technol 1999;53:3–10.
[45] Coelho MJ, Fernandes MH. Human bone cell cultures in biocompatibility testing. Part II: effect of ascorbic acid, beta-glycerophosphate and dexamethasone on osteoblastic differentiation. Biomaterials 2000;21(11):1095–102.
[46] Coombes AG, Rizzi SC, Williamson M, Barralet JE, Downes S, Wallace WA. Precipitation casting of polycaprolactone for applications in tissue engineering and drug delivery. Biomaterials 2004;25(2):315–25.
[47] Nimni ME. Polypeptide growth factors: targeted delivery systems. Biomaterials 1997;18:1201–25.
[48] Ingber DE. Mechanical and chemical determinants of tissue development. In: Lanza RP, Langer R, Vacanti J, editors. Principles of tissue engineering. San Diego: Academic Press; 2000. p. 101–10.
[49] Kunzler TP, Huwiler C, Drobek T, Vörös J, Spencer ND. Systematic study of osteoblast response to nanotopography by means of nanoparticle-density gradients. Biomaterials 2007;28:5000–6.
[50] Liao H, Andersson AS, Sutherland D, Petronis S, Kasemo B, Thomsen P. Response of rat osteoblast-like cells to microstructured model surfaces in vitro. Biomaterials 2003;24:649–54.